Annu. Rev. Biomed. Eng. 2002. 4:211–34
doi: 10.1146/annurev.bioeng.4.020702.153447

ELECTROMAGNETIC FIELDS: Human Safety Issues

Om P. Gandhi
Department of Electrical and Computer Engineering, University of Utah, Salt Lake City, Utah 84112-9206; e-mail: gandhi@ee.utah.edu

Key Words safety standards, internal EM fields, ELF to microwave frequencies, safety assessment and compliance testing

■ **Abstract** Most of the recently revised safety standards worldwide are set in terms of internal rates of electromagnetic energy deposition (specific absorption rates or SAR) at radio frequencies (RF) and microwave frequencies, and of induced electric fields or current densities at lower frequencies up to 10 MHz. Numerical methods have been developed that use millimeter resolution anatomically based models of the human body to determine SAR or the induced electric fields and current densities for real-life EM exposure conditions. A popular method for use at RF and microwave frequencies is the finite-difference time-domain method. This method is described and illustrated for SAR distributions due to cellular telephones for head models based on human anatomy. A method often used for calculations of induced electric fields and current densities at low frequencies is the impedance method. Use of this method is illustrated by an example of an electronic article surveillance (EAS) system for anatomic models of an adult and 10- and 5-year-old children. Experimental phantoms using a fluid to simulate the dielectric properties of the brain may be used for determination of peak 1- or 10-g SAR needed for compliance with the various safety standards.

CONTENTS

INTRODUCTION

Electromagnetic fields are being increasingly used for many new and rapidly expanding applications. In addition to the traditional uses from domestic electrical power to broadcasting to microwave radar, some of the newer applications are for wireless telephones and data links, electronic security systems, and many others. Hardly a year goes by without a new application of electromagnetic (EM) fields for use by the public. This also creates public concern about the safety of these EM fields.

Fortunately, there are expert committees in many countries that examine the human safety issues and suggest exposure levels that may not be exceeded. Most of the recently revised safety standards for exposure to electromagnetic fields are set in terms of limits of internal rates of electromagnetic energy deposition (specific absorption rates or SARs) at RF and microwave frequencies and of induced current densities for the various tissues at lower frequencies up to 10 MHz (1, 2). Since 1996, the U.S. Federal Communications Commission (FCC) has required wireless systems such as portable handsets, wireless laptops, and base stations to comply with radiofrequency radiation safety guidelines (3). Requirements for SAR certification for personal wireless devices and compliance with induced current density limits for low-frequency electronic article surveillance (EAS) systems (from a few Hz to a few MHz) are also being initiated in the European Union, Canada, Australia/New Zealand, Japan, and several other countries.

Over the past 30 years, increasingly sophisticated computational and experimental techniques have been developed for determination of SAR distributions or induced electric fields and current densities in anatomically based models of the human body with present-day voxel resolutions on the order of 1–3 mm (4–6).

We discuss the important computational and experimental techniques developed for bioelectromagnetic problems both for far-field and near-field exposures. We illustrate the use of these techniques to calculate currents induced in the human body by electromagnetic fields (EMFs) and for calculation of SARs by using examples of some recent applications such as safety compliance testing of microwave devices, e.g., handheld mobile telephones, and wireless laptops and base stations; and of low-frequency EAS systems.

SAFETY STANDARDS

The most commonly used safety standards at the present time are the ANSI/IEEE C95.1 (1) and ICNIRP (2). The basic restrictions for both of these standards are in terms of induced current density (or electric fields) at lower frequencies up

TABLE 1 ICNIRP basic restrictions for time-varying electric and magnetic fields for frequencies up to 10 GHz (2)*

Exposure	Frequency range	Current density J for head and trunk mA/m^2	Whole-body average SAR W/kg	Localized SAR for head and trunk W/kg	Localized SAR (limbs) W/kg
Occupational exposure	Up to 1 Hz	40	—	—	—
	1–4 Hz	$40/f$	—	—	—
	4 Hz–1 kHz	10	—	—	—
	1–100 kHz	$f/100$	—	—	—
	100 kHz–10 MHz	$f/100$	0.4	10	20
	10 MHz–10 GHz	—	0.4	10	20
General public exposure	Up to 1 Hz	8	—	—	—
	1–4 Hz	$8/f$	—	—	—
	4 Hz–1 kHz	2	—	—	—
	1–100 kHz	$f/500$	—	—	—
	100 kHz–10 MHz	$f/500$	0.08	2	4
	10 MHz–10 GHz	—	0.08	2	4

*Note: (*a*) f is the frequency in Hertz, (*b*) current densities J should be averaged over a cross section of 1 cm^2 perpendicular to the direction of induced current, and (*c*) localized SAR averaging mass is any 10 g of contiguous tissue.

to a few megahertz (MHz), and SARs at higher frequencies up to a few gigahertz (GHz). The basic restrictions for frequencies up to 10 GHz prescribed in the ICNIRP standard (2) are given in Table 1. The IEEE safety standard (1), on the other hand, is given in terms of maximum permissible exposures (MPE) of incident external fields for controlled and uncontrolled environments corresponding to occupational and general public exposures, respectively. The IEEE MPEs are given in Table 2 for controlled and uncontrolled environments, respectively. As for the ICNIRP standard, here too, the underpinning is in terms of whole-body average and localized SAR. For frequencies between 0.1 and 6000 MHz (6 GHz), the whole-body average SAR limits of 0.4 W/kg for controlled environments and 0.08 W/kg for uncontrolled environments are identical to those in the ICNIRP standard (see Table 1). In this same frequency range, the peak local SAR for any 1 g of tissue (defined as a tissue volume in the shape of a cube) should not exceed 8.0 and 1.6 W/kg for the head and trunk regions for controlled and uncontrolled environments, respectively. Both of these values are somewhat lower and only 80% of the peak local SARs of 10.0 and 2.0 W/kg suggested by ICNIRP for occupational and general public exposures, respectively. Another distinction between these two widely used safety standards is that whereas the peak SARs are to be calculated for any 1 g of tissue for the IEEE standard, a considerably larger averaging weight of 10 g of tissue is suggested by the ICNIRP standard for the tissues of the head and trunk. However, the peak local SARs for the limbs, i.e., arms and legs, are identical in both the IEEE and ICNIRP standards. The peak local 10-g averaged

TABLE 2 The IEEE maximum permissible exposure limits for controlled (occupational) and uncontrolled (general public) environments (1)*

	Controlled environments (Occupational)			Uncontrolled environments (General public)		
Frequency range MHz	**E V/m**	**H A/m**	**Power density mW/cm^2**	**E V/m**	**H A/m**	**Power density mW/cm^2**
0.003–0.1	614	163	—	614	163	—
0.1–3.0	614	$16.3/f$	—	614 (up to 1.34 MHz) $823.8/f$ (from 1.34–3.0 MHz)	$16.3/f$	—
3–30	$1842/f$	$16.3/f$	—	$823.8/f$	$16.3/f$	—
30–100	61.4	$16.3/f$	—	27.5	$158.3/f^{1.668}$	—
100–300	61.4	0.163	1.0	27.5	0.0729	0.2
300–3000	—	—	$f/300$	—	—	$f/1500$
3000–15,000	—	—	10	—	—	$f/1500$
15,000–300,000	—	—	10	—	—	10

* Note: f is the frequency in MHz.

SARs in both of the standards are 20.0 and 4.0 W/kg for occupational and general public exposures, respectively.

As seen in Table 1 for the ICNIRP standard, for low-frequency exposures up to 10 MHz, the basic restrictions are in terms of maximum induced current densities averaged over a cross section of 1 cm^2 perpendicular to the current direction. The maximum induced current density limits are not as clearly spelled out in the IEEE standard where the MPEs are instead given in terms of maximum allowable currents through arms and legs for controlled and uncontrolled environments, respectively. This difference may, however, be narrowed in the future, because a planned revision of the IEEE standard will prescribe maximum induced electric fields for the various regions of the body.

The IEEE standard is used in the United States and a slightly modified version is used in Canada. The ICNIRP standard is used in the European Union and slightly altered versions of this standard are used in Australia/New Zealand, Japan, and Korea. In any case, from the discussion of this section, it is clear that safety assessment of the various electromagnetic devices or environments involves determination of induced electric fields or current densities at low frequencies up to a few MHz and of whole-body average and peak 1- or 10-g tissue-averaged SARs at the higher frequencies.

COMPUTATIONAL TECHNIQUES FOR RF/MICROWAVE FREQUENCIES

The FDTD Method with Uniform and Expanding Grid

The finite-difference time-domain (FDTD) method is extremely versatile for bioelectromagnetic problems. FDTD has been used for modeling whole-body or partial-body exposures due to spatially uniform or nonuniform near- or far-fields that are sinusoidally varying or transient in nature (4, 7–11). The latter includes the fields associated with an electromagnetic pulse (EMP).

In this method, the time-dependent Maxwell's equations, given by

$$\nabla \times \mathbf{E} = -\mu \frac{\partial \mathbf{H}}{\partial t} \tag{1}$$

and

$$\nabla \times \mathbf{H} = \sigma \mathbf{E} + \varepsilon \frac{\partial \mathbf{E}}{\partial t}, \tag{2}$$

are implemented for a lattice of subvolumes or Yee space cells that may be cubical or parallelepiped with different dimensions Δx, Δy, and Δz in the x, y, and z directions, respectively. The components of **E** and **H** are positioned about each of the cells at half-cell intervals and calculated alternately (leapfrogged) with half-time steps, $\Delta t/2$. The details of the method are given in several of the above-referenced publications and books (12, 13) and are, therefore, not repeated here.

In the FDTD method, it is necessary to represent not only the scatterer/absorber such as the human body or a part thereof, but also the electromagnetic sources, including their shapes, excitations, and so forth, if these sources are in the near-field region. On the other hand, the far-field sources are described by means of incident plane-wave fields specified on a three-dimensional source "box" located typically 6 to 10 cells away from the exposed body. The interaction space consisting of several hundred thousand to several million Yee cells is truncated by means of absorbing boundaries. The penetrating fields are tracked in time for all cells of the interaction space. The computation is considered to be completed when either the **E** and **H** fields have died off for an impulsive excitation or, for a sinusoidal excitation, when the sinusoidal steady-state is observed for all cells within the interaction space.

Even though a uniform FDTD grid has mostly been used for the bioelectromagnetic problems, an expanding-grid formulation has also been proposed by Gao & Gandhi (14). For near-field sources, this offers the advantage of modeling the tightly coupled regions such as the ear and the proximal side of the head with a fine resolution (small cell size) while allowing cell sizes to increase gradually as one moves further away from the regions of primary interest. The expanding-grid algorithm allows different cell-to-cell expansion factors along the three coordinate axes, and can reduce by a factor of 4 to 10 the total number of cells needed to

model a given volume as compared to a uniform grid formulation wherein the cells with the finest resolution are used throughout the volume. Some of the applications to date are for calculations of induced current and SAR distributions for a worker model exposed to an RF dielectric heater (15) and for SAR distributions due to cellular telephones (16, 17). Another potential application is for dosimetry of the human body at higher frequencies where the interior of the exposed body is relatively shielded and may, therefore, be modeled with coarser cells or ignored altogether. For all of these applications the coupled fields diminish rapidly into the exposed parts of the body. By using smaller cell sizes on the order of 1 mm for the coupled region, one can determine the SARs with higher precision and better model the irradiating source as well (for example, the personal wireless device, its antenna, and the feed region).

A variation of the expanding-grid formulation is the use of subgridding (18). Whereas a slowly expanding cell size with cell-to-cell expansion factors on the order of 1.1 to 1.25 are used in the expanding-grid formulation, a stepped expansion factor of two, and at times three, may be used in the subgridding method to represent the regions where the electromagnetic coupling is considerably lower.

COMPUTATIONAL TECHNIQUES FOR LOW FREQUENCIES

For exposures to EMFs from low-frequency sources such as power lines at 50/60 Hz, induction heaters and EAS devices in the kilohertz to megahertz range, etc., several numerical techniques have been developed (4, 19–33). These methods are the admittance and impedance methods (19–23), the finite-element method (25), the scalar potential finite-difference (SPFD) method (27–29), and the finite-difference time-domain method with frequency scaling (24, 26, 30). At low frequencies, it is possible to treat exposure to electric and magnetic fields separately and the induced electric fields or current densities added vectorially for each of the voxels (21, 31). Using anatomically based models with voxel resolutions of 1–6 mm, these methods have been used to calculate the induced electric fields and current densities for the various regions of the body. For lack of space, we describe only one of these methods and its application to a recent problem of great interest, namely, compliance testing of electronic article surveillance (EAS) systems, in detail here.

The Impedance Method

First postulated in 1984, the impedance method (4, 20–23, 32, 33) has been found to be highly efficient as a numerical procedure for calculations of induced current densities and/or electric fields for exposure to low-frequency EM fields. Using tissue-classified anatomically based models with resolutions of 1 to 6 mm, some of the applications of this method are calculation of SAR distributions for operator exposure to nonuniform magnetic fields of induction heaters (22), induced current

densities and SARs due to capacitive-type electrodes used for hyperthermia (23), currents induced in the human body by electric and magnetic fields of electric blankets (4), current densities and electric fields induced by magnetic fields of EAS systems (33), etc.

In this method, the biological body or an exposed part thereof is represented by a three-dimensional (3D) network of impedances whose individual values are obtained from the complex conductivities ($\sigma + j\omega\varepsilon$) for the various locations of the body. The impedances for various directions for the three-dimensional network can be written as

$$Z_m^{i,j,k} = \frac{\delta_m}{\delta_n \delta_p \left(\sigma_m^{i,j,k} + j\omega\varepsilon_m^{i,j,k}\right)}, \tag{3}$$

where i, j, and k indicate the voxel index; m is the direction, which can be x, y, or z, for which the impedance is calculated; $\sigma_m^{i,j,k}$ and $\varepsilon_m^{i,j,k}$ are the conductivities and the electrical permittivities for the voxels i, j, and k; δ_m is the thickness of the cell in the mth direction; and δ_n and δ_p are the widths of the voxel in directions at right angles to the mth direction.

In the impedance method formulation, it can be seen that the cells need not be identical so that fairly thin features of the body can be modeled as well as the interfaces between the various tissues and organs. Also, the dielectric properties (σ, ε) for a given cell can be directionally dependent.

A recent application of this method is for calculation of induced electric fields and current densities for exposure to nonuniform vector magnetic fields of EAS systems (33). Because of the relatively new and rapidly expanding use of the magnetic fields for security systems such as EAS and radiofrequency identification (RFID) systems (34) and the need for safety compliance testing of such devices (35), this application is discussed in detail in this article.

SOME APPLICATIONS OF NUMERICAL TECHNIQUES

SAR Distributions Due to Cellular Telephones

The finite-difference time-domain technique has been used by many authors to calculate SAR distributions and radiation patterns of cellular telephones held close to the head (4–6, 36–43). It is possible to use CAD-derived models of cellular telephones in order to represent the detailed construction of the telephone more accurately. An illustration of two CAD-derived telephones, one each at 835 and 1900 MHz, is given in Figure 1 (40, 41). The anatomic model resolutions used by various authors are typically on the order of 1–3 mm. The calculated energy depositions are highly superficial with penetration depths on the order of 3–5 cm for the side of the head close to the radiating antenna. Shown in Figures 2*a* and 2*b* are two views of the calculated SAR distributions for a $1.974 \times 1.974 \times 3$ mm resolution anatomic model of the human head for a cellular telephone radiating 600 mW of power at 835 MHz. This is the maximum power

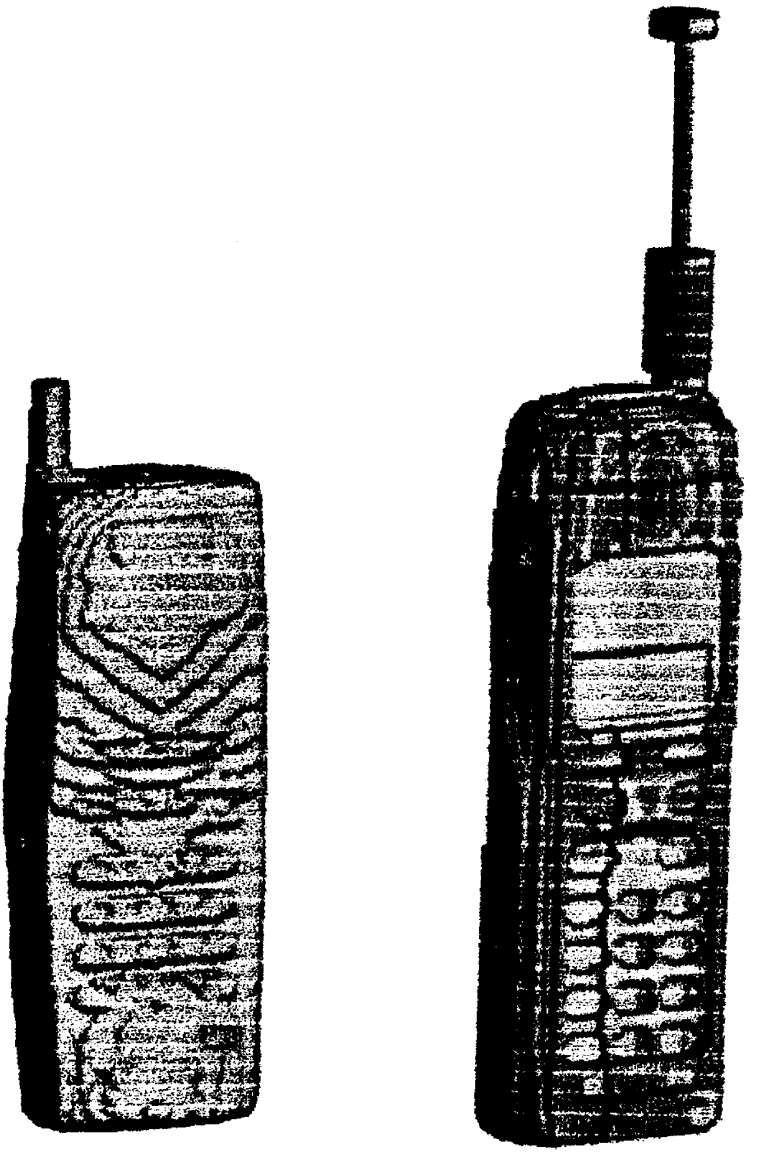

(a) 835 MHz model (b) 1900 MHz model

Figure 1 An illustration of two CAD-derived telephones used for SAR calculations.

radiated by a cellular telephone in the analog AMPS mode. For calculations of SAR distributions, several numerical codes are presently available commercially so that they may be used to design a telephone that meets the SAR safety guidelines and gives desirable radiation patterns.

Because different anatomic models of the human head have been used by various authors, the calculated SAR distributions are slightly different with peak 1-g SARs that may be up to 50% different even when identical antenna lengths and slant angles of the telephones vis à vis the head are used (43). This variation in the calculated peak 1-g SAR may be reduced somewhat if care is taken in accurately positioning the telephone relative to the ear. In one such study, the effect of using different anatomical models of the head on SAR distributions is examined (40). For this study, two different anatomically based models of the human head and neck derived from the MRI scans of two adult male volunteers are used. The first of these models, described in detail in Reference (5), has a resolution of $1.974 \times 1.974 \times 3.0$ mm. The second anatomic model, described in Reference (40), has a resolution of 0.9375 mm for each of the cubical voxels and is based on the head of a second individual. The head and neck parts of each of the models have been segmented into 15 tissue types: muscle, fat, bone (skull), cartilage, skin, nerve, blood, parotid gland, eye humor, sclera and lens, CSF, brain, and pineal and pituitary glands. Appropriate mass densities and dielectric properties depending on the irradiation frequency, listed in (5, 40), were used to calculate SAR distribution using the FDTD method. The SAR results given in Table 3 use three different models: Model A, with a resolution of $1.974 \times 1.974 \times 3$ mm; its resampled version, with a resolution

TABLE 3 SAR distributions for three anatomic models of the human head for a cellular telephone of handset dimensions $2.2 \times 5.0 \times 15.6$ cm. Frequency = 1900 MHz, radiated power = 125 mW

	Model A $\mathbf{1.974 \times 1.974 \times 3.0}$ **mm**	**Model B** $\mathbf{0.987 \times 0.987 \times 1.0}$ **mm (resampled from Model A)**	**Model C** $\mathbf{0.9375\ mm^3}$
Peak 1-voxel SAR (W/kg)	5.88	10.97	6.77
Peak 1-g SAR (W/kg)	1.58	1.62	1.41
Peak 1-g SAR for brain (W/kg)	0.27	0.26	0.32
Power absorbed by head, neck and hand	58%	61.7%	61.5%
Brain average SAR (mW/kg)	9.33	9.33	12.31
CSF average SAR (mW/kg)	10.08	10.10	8.68
Lens average SAR (mW/kg)	1.17	1.17	1.61
Sclera average SAR (mW/kg)	1.41	1.44	2.50
Humor average SAR (mW/kg)	2.40	2.39	3.21

of $0.987 \times 0.987 \times 1$ mm (Model B); and a new 0.9375-mm resolution model (Model C). Given in Table 3 are the salient features of the calculated SARs and the powers absorbed for the various regions of the head for Models A, B, and C for a cellular telephone of handset dimensions $2.2 \times 5.0 \times 15.5$ cm. Used for the SAR calculations is a handset with a quarter-wavelength (3.95 cm)-long antenna radiating a time-averaged power of 125 mW (peak pulses of power output 1W with a duty cycle of 1/8) at 1900 MHz. As expected, the SAR distributions for Models A and B with different resolutions, but derived from the anatomic model of the same head, are very similar. The SARs calculated for Model C, which was derived for a different individual, are slightly different, but the peak 1-g SAR needed for compliance testing against the ANSI/IEEE and FCC guidelines (1, 3) is still within approximately 15% of that derived for Models A and B.

Another useful comparison is that for peak 1- and 10-g SARs needed for compliance testing against the ANSI/IEEE and FCC guidelines used in the United States (1, 3) and against the ICNIRP Standard (2) used by the European Union Countries, respectively. Given in Table 4 is the comparison of the peak 1- and 10-g SARs for various tilt angles of the cellular telephone handset of dimensions $2.96 \times 5.73 \times 15.5$ cm vis à vis the head (Model A). Assumed for the calculations are the quarter-wave monopole antennas of lengths 9.0 and 3.95 cm for this handset at 835 and 1900 MHz, respectively. It is interesting to note that peak 1-g and 10-g SARs generally diminish with increasing tilt angle both at 835 and 1900 MHz. It should also be noted that the peak 10-g SARs required for compliance testing against the ICNIRP standard (2) are a factor of two or more times lower than the peak 1-g SARs needed for compliance testing by the FCC in the United States (3).

TABLE 4 Peak 1- and 10-g average SARs for various tilt angles (actual tissue weights in parentheses). Assumed for SAR calculations is a handset of dimensions $2.96 \times 5.73 \times 15.5$ cm using quarter-wave monopole antennas of lengths 9.0 or 3.95 cm at 835 or 1900 MHz, respectively (41)

	835 MHz (600 mW)		**1900 MHz (125 mW)**	
Tilt angle	**1 g SAR W/kg**	**10 g SAR W/kg**	**1 g SAR W/kg**	**10 g SAR W/kg**
0°	2.93 (1.01 g)	1.41 (10.19 g)	1.11 (1.03 g)	0.59 (10.08 g)
20°	2.7 (1.00 g)	1.33 (10.00 g)	1.08 (1.01 g)	0.56 (10.06 g)
30°	2.44 (1.03 g)	1.21 (10.18 g)	1.08 (1.03 g)	0.57 (10.00 g)
45°	2.14 (1.00 g)	1.1 (10.07 g)	0.85 (1.01 g)	0.42 (10.07 g)
30° + 9° rotation toward the mouth	2.31 (1.10 g)	1.08 (10.05 g)	1.20 (1.01 g)	0.44 (10.11 g)

Furthermore, because the peak 10-g SAR limit in the ICNIRP standard is 2.0 W/kg as opposed to 1.6 W/kg in the FCC standard, the radiated power allowed by the ICNIRP standard (2) would be almost 2.5 times higher than that allowed by the IEEE or FCC standards (1, 3).

Induced Electric Fields, Current Densities, and SARs for EAS and RFID Systems

Electronic article surveillance (EAS) and RF identification (RFID) systems based on the use of alternating magnetic fields at frequencies from 50/60 Hz up to 10–15 MHz are being rapidly introduced into society to prevent unauthorized removal of items from stores, libraries, and hospitals or for RF detection of identification cards to control access (34). The EAS and RFID systems may take the form of one- or two-sided panels of current-carrying loops or pillars at or near the exit door, or loops hidden in the ceiling and/or the mat on the floor. Another manifestation is the magnetic tag deactivation systems that are mounted as checkout countertop devices. The net result is that an individual passing through or standing close to these devices is exposed to nonuniform vector magnetic fields emanating from these EAS and RFID systems.

As mentioned earlier, limits of induced current densities and SARs in the human body have been prescribed in the IEEE and ICNIRP standards (1, 2) that may not be exceeded for exposure of the general public or for occupational situations. The basic restrictions specified in the ICNIRP guidelines (see Table 1) are to limit the induced current densities for the central nervous system (CNS) tissues, e.g., the brain and the spinal cord for frequencies up to 100 kHz; current densities as well as SARs for frequencies between 100 kHz and 10 MHz; and only SARs (both whole-body-average and peak local 10-g SARs) for frequencies above 10 MHz. The European Standard EN50357 for compliance testing of EAS and RFID systems defines the procedures to be used for evaluation of human exposure to electromagnetic fields of these systems (35). Because experimental compliance testing is tedious, computational methods using heterogeneous anatomically based models of the human body may be used to show compliance of the new EAS devices.

For this application (33), a full $1.974 \times 1.974 \times 2.93$-mm resolution model of the adult male described in Reference (4) is used. Also used are scaled models of the 10- and 5-year-old children, derived from the model of the adult using the external dimensions typical of the children (see Table 5). From Geigy Scientific Tables (44), the head circumference does not change much from a 5-year-old child to an adult (approximately 5.5%) even though the surface area increases by approximately 33% and body height and weight increase significantly. Some typical external dimensions and derived voxel sizes for anatomic models of the male adult and 10- and 5-year-old boys are given in Table 5. The three models used for the calculations of different heights and weights but fairly similar circumferences of the head are visualized in Figure 3. Because of the fairly large size of the models with a grid

TABLE 5 Some typical external dimensions and derived voxel sizes used for the anatomic models of the male adult and 10- and 5-year-old boys (33)

	Adult male	**10-year-old boy**	**5-year-old boy**
Head circumference[a] (cm)	53.8	52.3	51.0
Body weight[a] (kg)	71.7	30.5	18.9
Height[a] (cm)	176	138	112
Body surface area[a] (cm^2)	17,400	9610	7510
Head surface area[a] (cm^2)	1305	1048	984
Voxel size for head (mm)	$1.974 \times 1.974 \times 2.930$	$1.974 \times 1.974 \times 2.352$	$1.871 \times 1.871 \times 2.330$
Voxel size for arms, torso, and legs (mm)	$1.974 \times 1.974 \times 2.930$	$1.400 \times 1.400 \times 2.282$	$1.196 \times 1.196 \times 1.782$

[a]See Reference (44).

size of $256 \times 151 \times 602$ or approximately 23.3 million voxels, a Sun Microsystems UltraSparc II work station is used for the calculations of the induced electric fields from which the induced current densities are calculated using the tissue-dependent conductivities for each of the voxels. The problem requires a computer memory of 1.18 Gigabytes.

An EAS System

Even though the induced electric fields and current densities have been evaluated for several EAS device geometries mentioned in the previous section, we give details for only one such system here because of lack of space. A pass-by system assumed here is a 30-kHz one-sided EAS system consisting of two rectangular coils, each of width 50 cm and height 60 cm with an overlap of 10 cm, carrying in-phase currents of 100 A turns rms for each of the coils (33). This system is sketched in Figure 4. The dimensions and frequency used for this system are made up to illustrate the procedure and, to our knowledge, are not representative of any commercial products. This is done to protect the proprietary interests of the manufacturers. Using Biot-Savart's law of electromagnetics, a computer program is written to calculate the rms values of the magnetic fields B_x, B_y, and B_z for the locations close to the assumed EAS system that are likely to be occupied by the various parts of the human. The calculated variations of the magnetic field components and the total magnetic field,

$$B_{total} = \left(B_x^2 + B_y^2 + B_z^2\right)^{1/2}, \tag{4}$$

is sketched in Figure 5 for an imaginary vertical line that is centrally located ($y = 0$) at a distance $x = 20$ cm from the plane of the EAS panel. This is because of the placement of the human model such that this vertical line passes through the armpit

(*a*) Adult male. (*b*) Model of 10-year-old boy. (*c*) Model of 5-year-old boy.

Figure 3 The three anatomic models used for calculations of induced electric fields and current densities.

tangential to the proximal side of the torso recommended by European Standard EN50357 (35) for compliance testing against ICNIRP guidelines.

From Figure 5 we can see that the magnetic fields are the highest for the region of the brain $100.2 < z < 111.2$ cm for the model of the 5-year-old, intermediate for the model of the 10-year-old ($125.8 < z < 137.2$ cm), and lowest for the model of the adult ($161.2 < z < 175.4$ cm), respectively. As seen from Figure 5, the total magnetic field for the brain may be four to five times higher for the model of a 5-year-old child and two to three times higher for the model of a 10-year-old child as compared to that for an adult, respectively. For the spinal cord, the vertical coordinate z is between 60.6 and 100.2 cm for the 5-year-old, between 77.6 and 125.8 cm for the 10-year-old, and between 99.6 and 161.2 cm for the model of the adult. Here, too, the magnetic fields are higher for the regions of the spinal cord for both of the models of the children as compared to those for the model of the adult.

The impedance method is used to calculate the induced electric fields and current densities for every voxel of the three models shown in Figure 3 with the proximal side of the torso at a distance of 20 cm from the yz plane passing through the

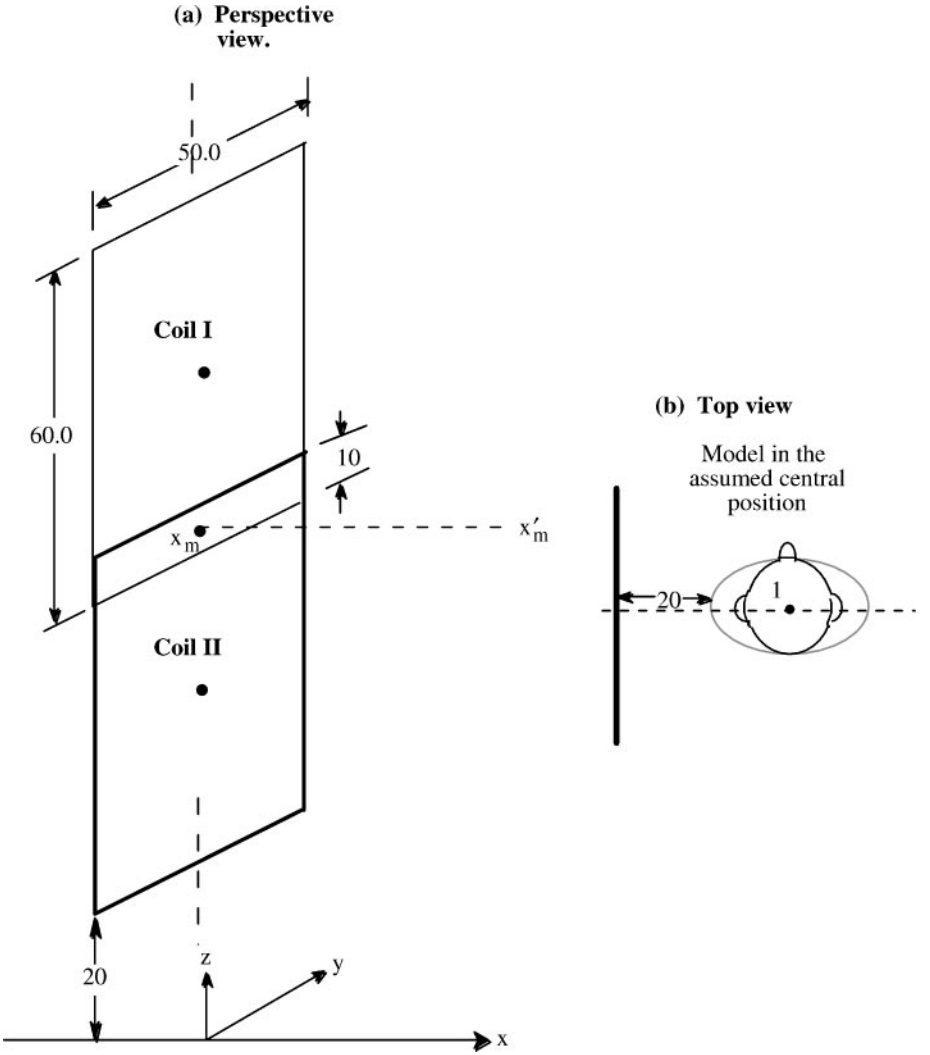

Figure 4 An assumed EAS system using a pair of rectangular coils with an overlap of 10 cm. The lower rung of the bottom coil is assumed to be 20 cm off the ground plane. The marked dimensions are in cm.

EAS coils as suggested in EN50357 Standard (35). From the component values of the x-, y-, or z-directed induced current densities J_x, J_y, and J_z, respectively, the total current densities (J) for each of the voxels are calculated using the following equation:

$$J = \left(J_x^2 + J_y^2 + J_z^2\right)^{1/2}. \tag{5}$$

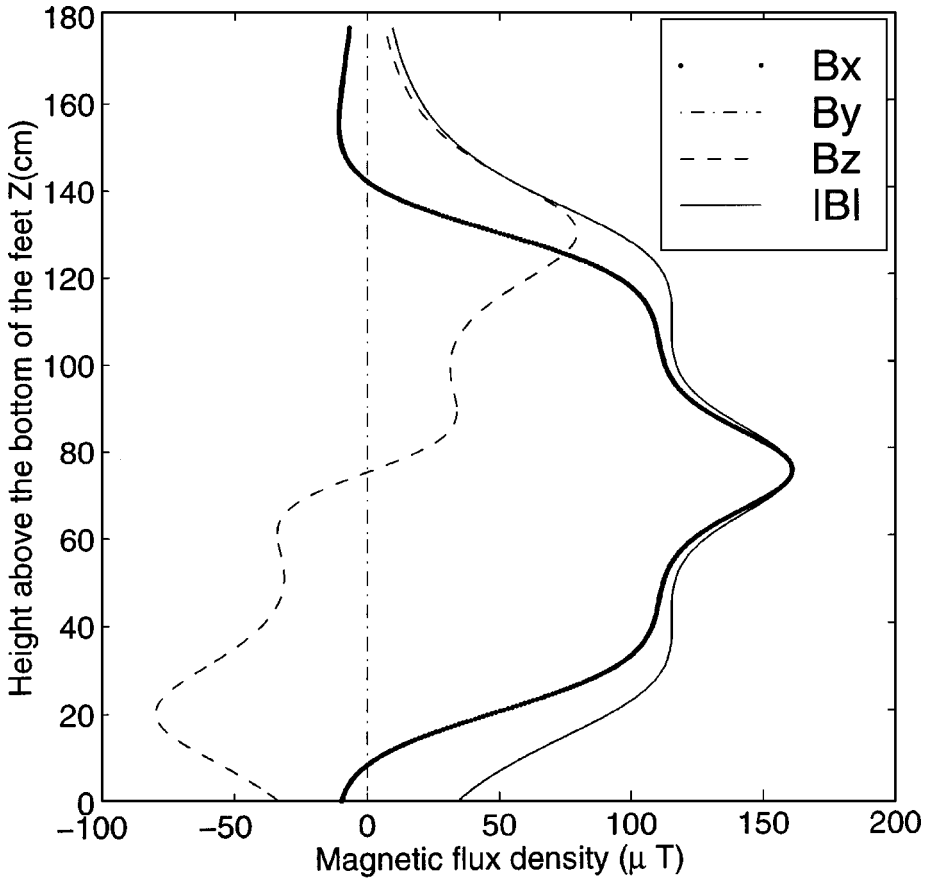

Figure 5 The calculated variation of the magnetic fields for a centrally located vertical line ($y = 0$) at a distance $x = 20$ cm from the plane of the EAS panel (see Figure 4).

The calculated organ-averaged and maximum 1 cm^2 area-averaged induced electric fields and current densities for the three human models for the pass-by EAS system of Figure 4 are given in Table 6. The maximum 1 cm^2 area-averaged current densities J_{max} for the brain and the spinal cord are considerably lower than the ICNIRP basic restriction at 30 kHz of 60 mA/m^2 for the general public for the model of the adult (see Table 1). Because of the shorter heights of the 10- and 5-year-old children, the brains of these models are in higher magnetic fields (see Figure 5), which results in the maximum current density for the 10-year-old model (64.6 mA/m^2) being close to the ICNIRP limit and that for the 5-year-old model (98.9 mA/m^2) being almost 65% higher than the ICNIRP limit of 60 mA/m^2 at 30 kHz. This is understandable because the average magnetic field for the region of the brain is about four times higher for the model of the 10-year-old and about

TABLE 6 The calculated organ-averaged and maximum 1 cm^2 area-averaged electric fields (E) and current densities (J) for the models of the adult and 10- and 5-year-old children for the 30 kHz magnetic panel type EAS system (33)

		Adult		10-year-old		5-year-old	
Organ		**J (mA/m^2)**	**E (mV/m)**	**J (mA/m^2)**	**E (mV/m)**	**J (mA/m^2)**	**E (mV/m)**
Brain	Organ-averaged	4.75	47.89	23.20	234.13	40.70	410.71
	max. (1 cm^2)	17.63	177.83	64.64	652.23	98.93	998.27
Pineal gland	Organ-averaged	0.92	9.29	17.42	175.73	36.27	365.95
	max. (1 cm^2)	—	—	—	—	—	—
Spinal cord	Organ-averaged	—	—	—	—	—	—
	max. (1 cm^2)	32.64	538.61	40.19	663.20	43.71	721.29
Heart	Organ-averaged	92.69	185.39	120.08	240.16	130.33	260.66
	max. (1 cm^2)	234.69	469.38	296.86	593.71	316.80	633.59
Liver	Organ-averaged	18.15	277.56	23.63	361.24	24.66	377.11
	max. (1 cm^2)	86.68	1325.33	114.57	1751.76	121.11	1851.78
Kidneys	Organ-averaged	36.41	239.41	38.06	250.23	38.05	250.19
	max. (1 cm^2)	88.08	579.09	81.26	534.26	78.07	513.26
Bladder	Organ-averaged	85.11	394.75	86.84	402.80	68.55	317.93
	max. (1 cm^2)	234.21	1086.33	222.24	1030.81	170.34	790.09
Pancreas	Organ-averaged	28.61	188.08	38.64	254.02	46.72	307.19
	max. (1 cm^2)	86.33	567.63	94.74	622.87	85.43	561.64

five to six times higher for the model of the 5-year-old as compared to that for the adult, respectively.

ASSESSMENT OF PERSONNEL SAFETY

As mentioned previously, most of the recently revised safety limits are set in terms of the SAR limits for RF/microwave frequencies (see Table 1). Because procedures to ascertain compliance with SAR limits are cumbersome, requiring computer modeling with large memory workstations, or bulky, mostly homogeneous experimental phantoms (45), they are ignored in favor of easy-to-measure incident fields (see Table 2). RF/microwave environments such as wireless base stations, broadcast installations, and industrial and medical equipment are thus erroneously declared safety compliant or not, based solely on the measured incident fields. Of particular interest at the present time is the tremendous proliferation of wireless base stations, especially in metropolitan and urban settings. Some methods have been developed for assessing personnel safety that may be of concern for regions close to such base stations where electromagnetic fields can be fairly high (42, 46). A relatively simple method that may be used for this and other near-field EM environments is the so-called spatial components method (46).

The Spatial Components Method

In this method, the vertical and horizontal components of the electric field are measured for an imaginary vertical (xz) plane ($0 \leq x \leq A$; $0 \leq z \leq B$), but without the human. This so-called plane of incidence is taken to be in the immediate vicinity of the intended location of the model of the human. The measured distributions for vertical- and horizontal electric field components E_z and E_x, respectively, are then expressed in terms of space harmonics as follows:

$$E_z = \sum_{m,n=0}^{\infty} C_{mn} \cos \frac{m\pi x}{A} \cos \frac{n\pi z}{B} \tag{6}$$

$$E_x = \sum_{m,n=0}^{\infty} D_{mn} \cos \frac{m\pi x}{A} \cos \frac{n\pi z}{B}, \tag{7}$$

where m and n are integers 0, 1, 2 . . ., and the space harmonics are defined over the plane of incidence of dimensions A and B along horizontal (x) and vertical (z) directions, respectively. All of the components with magnitudes C_{mn} and D_{mn} that are 10% or larger than the maximum amplitude are included for truncated versions of Equations 6 and 7, respectively.

By defining the origin ($x = 0$, $z = 0$) at either the upper or lower corner rather than at the center of the measurement plane, one can express any general variation of the fields even though cos ($m\pi x/A$) cos ($n\pi z/B$)-type modal terms are considered. Because the EM fields beyond about two times the horizontal extent of the human body and 1.25 times the human height have been shown to have minimal coupling to the human, the dimensions A and B are taken to be 0.96 m and 2.28 m, respectively. The spatial harmonics components method relies on the pre-stored solutions for the internal E-fields (E_x, E_y, E_z) for the various voxels of the human body model to different space harmonics that may be added depending upon the magnitudes and phases of the various space harmonic components obtained on-site for the measured electric field distributions.

The applicability of this technique for on-site dosimetry has been validated by comparing the SAR distributions obtained for near-field regions of some commercial base station antennas at 835 and 1900 MHz with those obtained by using the conventional FDTD method (46). Like the ray-tracing method used in Reference (42), because the measured electric field distributions for the commercial base station antennas were not readily available, the calculated field distributions in front of these transmitters were obtained using the FDTD method with a grid size of 3 cm at 835 MHz and 1.5 cm at 1900 MHz. Given in Figures 6 and 7 are two representative cases of human exposure in front of some typical base stations. In both of the figures, the calculated layer-averaged SARs using the spatial harmonic components method are compared with those obtained by the full FDTD method. Six components were found to be adequate at 835 MHz (Figure 6), whereas 10 components were needed at 1900 MHz (Figure 7) to obtain a very good agreement of the SAR distributions with those obtained using the full FDTD method.

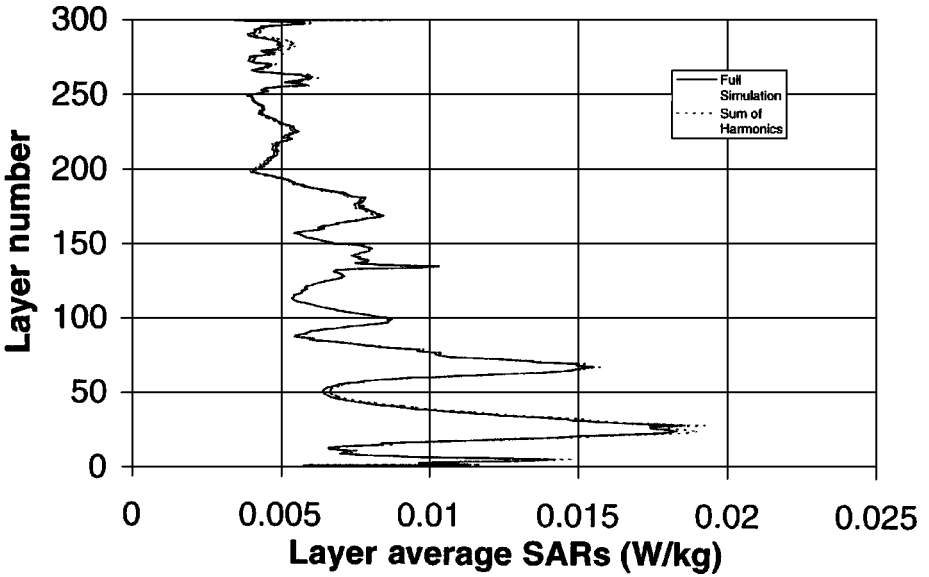

Figure 6 The calculated layer-averaged SAR distribution for the model of the human body due to a base station antenna made of an 18-cm-tall vertical dipole in front of a flat reflector of dimensions 24 × 24 cm. Frequency = 835 MHz, radiated power = 10 W, distance to the front plane of the model = 2 m.

Comparison of the calculated whole-body-average and peak 1-g SARs for the three base stations for different spacings to the human model are given in Tables 7 and 8, respectively. The whole-body-average and peak 1-g SARs are less than 5 to 10 percent different than those obtained using the full FDTD simulation. This is remarkable because the harmonic components method takes less than one minute on a portable PC whereas the full FDTD simulation takes over an hour of computer time using the same PC.

EXPERIMENTAL TECHNIQUES FOR SAFETY ASSESSMENT

Experimental determination of SAR or induced electric fields or current densities at lower frequencies is very cumbersome for use in the field for real-life exposure situations. Whole-body phantoms made of plastic human-shaped bags (45) filled with homogenous gels representing the average of electrical properties of human tissues (dielectric constants and conductivities) are not very portable and certainly are incapable of providing information on SAR distributions. Experimental dosimetry for cellular telephones held against models of the head is more advanced, and automated SAR measurement systems have been set up for determination of the 1- and 10-g peak SARs needed for compliance testing of personal

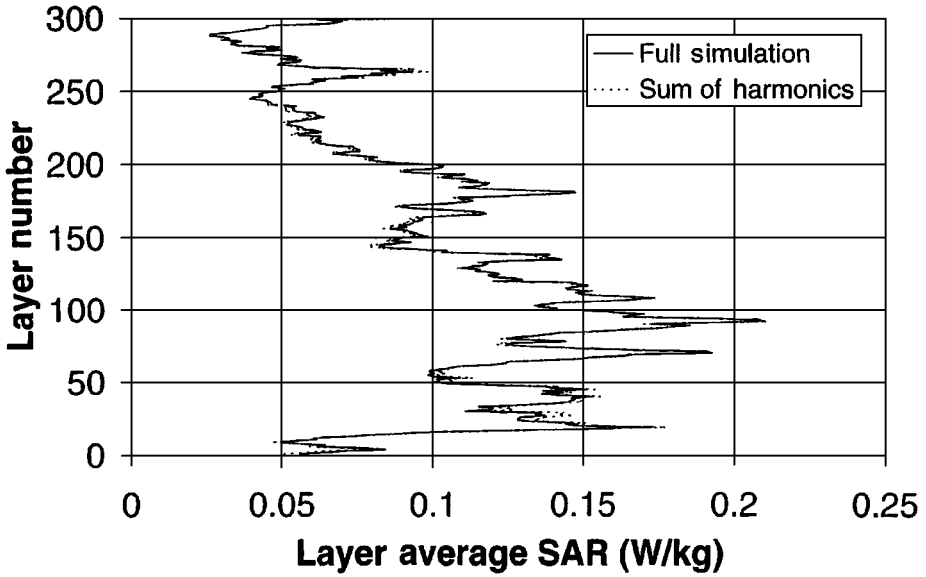

Figure 7 The calculated layer-averaged SAR distribution for the model of the human body due to an aperture type base station antenna of dimensions 38.1×20.3 cm along vertical and horizontal directions, respectively. Frequency = 1900 MHz; radiated power = 120 W, distance to the front plane of the model = 3 m.

wireless devices (47–49). Shown in Figure 8 is an automated SAR measurement system used for validation of the calculated SAR distributions for tissue-simulant phantoms in the shapes of a rectangular box and a sphere and for compliance testing of personal wireless handsets both at 835 and 1900 MHz (49). The setup uses a 3D stepper motor system to move a Narda Model 8021 E-field probe to measure the SAR distribution inside a canonical model or a head-shaped brain-simulant phantom near the radiating device. The head and neck part of the model is made of an outer shell 5–7-mm thick (except for the region of the pinna that is thinner and about 2–3 mm) of epoxy laced with a KCℓ solution for losses (50). This and the upper part of the torso are filled with brain-simulant fluids with measured electrical properties (dielectric constant and conductivity) that are similar to those for the brain at the center frequencies of interest (835 and 1900 MHz) (49).

The accuracy of the automated setup shown in Figure 8 has been validated by comparing the measured and the FDTD-calculated SAR distributions for tissue-simulant phantoms of canonical shapes such as a rectangular box and a sphere and by testing a number of telephones, including some research test samples from diverse manufacturers, at 835 and 1900 MHz, respectively (49). Table 9 gives the comparison of the numerical and measured peak 1-g SARs for these devices using the head-shaped experimental phantom model and the uniform-grid FDTD

TABLE 7 Comparison of whole-body-average SARs and peak 1-g SARs obtained for various distances of the model from a base station at 824–849 MHz using the full FDTD simulation and the spatial harmonic components method (46)*

	Whole-body average SAR			Peak 1-g SAR		
Distance (m)	Full FDTD simulation (W/kg)	Harmonic components method (W/kg)	% difference	Full FDTD simulation (W/kg)	Harmonic components method (W/kg)	% difference
0.5	0.033	0.033	2.50	2.76	2.85	−3.38
0.765	0.023	0.023	0.00	1.69	1.73	−2.21
1	0.017	0.017	1.35	1.11	1.13	−1.65
2	0.006	0.006	0.09	0.38	0.36	4.41

*Assumed is a base station antenna using an 18-cm tall vertical dipole in front of a flat reflector of dimensions 24 × 24 cm (see Figure 6 for layer-averaged SAR distribution).

numerical procedure used for calculations of SAR distributions for the anatomically based Model A of the head of an adult male with a resolution of 1.974 × 1.974 × 3.0 mm. The measured and the calculated SARs for the tested telephones, which have quite different operational modes (AMPS, TDMA, CDMA, etc.) and antenna structures (helical, monopole, or helix-monopole), vary from 0.13 to 5.41 W/kg. It is recognized that only the AMPS telephones may use time-averaged powers as high as 600 mW, whereas the telephones using TDMA and CDMA would typically use 200–300 mW of time-averaged power. Because several of these telephones were capable of operating in dual modes such as AMPS and CDMA, all of the 1-g SARs given for 835 MHz are normalized to the higher possible time-averaged power of 600 mW. Even though widely different peak 1-g SARs were

TABLE 8 Comparison of whole-body-average SARs and peak 1-g SARs obtained for various distances of the model from a base station antenna at 1850–1910 MHz using the full FDTD simulation and the spatial harmonic components method (46)*

	Whole-body average SAR			Peak 1-g SAR		
Distance (m)	Full FDTD simulation (W/kg)	Harmonic components method (W/kg)	% difference	Full FDTD simulation (W/kg)	Harmonic components method (W/kg)	% difference
1	0.029	0.028	3.04	21.68	21.36	1.46
3	0.088	0.087	1.30	5.03	4.95	1.67
5	0.036	0.036	−1.65	2.48	2.42	2.33

*Assumed is an aperture type base station antenna of dimensions 38.1 × 20.3 cm radiating 120 W of power (see Figure 7 for layer-averaged SAR distribution).

TABLE 9 Comparison of the measured and FDTD-calculated peak 1-g SARs for a number of wireless devices, five each at 835 and 1900 MHz, respectively (49)

	Mobile telephones at 835 MHz		
	Time-averaged radiated power mW	**Experimental method W/kg**	**Numerical method W/kg**
Telephone A	600	4.02	3.90
Telephone B	600	5.41	4.55
Telephone C	600	4.48	3.52
Telephone D	600	3.21	2.80
Telephone E	600	0.54	0.53
	PCS telephones at 1900 MHz		
Telephone A′	125	1.48	1.47
Telephone B′	125	0.13	0.15
Telephone C′	125	0.65	0.81
Telephone D′	125	1.32	1.56
Telephone E′	99.3	1.41	1.25

obtained because of the variety of antennas and handsets, agreement between the calculated and the measured data was excellent and generally within $\pm 20\%$ or ± 1 dB (49). This is remarkable because an MRI-derived, 15-tissue anatomically based model of the adult human head (Model A) was used for FDTD calculations and a relatively simplistic two-tissue phantom model was used for experimental peak 1-g SAR measurements.

CONCLUSIONS AND FUTURE DIRECTIONS

Dosimetry for electromagnetic fields from very low frequencies to microwave frequencies has advanced considerably over the past 15–20 years. Development of highly efficient numerical techniques makes it possible to get distributions of internal electric fields for SARs or for induced current densities for anatomically realistic models of the human body with whole-body resolutions on the order of 1–2 mm and part-body resolutions of submillimeter voxel sizes. All of these techniques have been developed and tested for relatively uniform far-fields or highly nonuniform near-field sources. For personal wireless devices such as cellular telephones, source-body coupling is important and has been included by solving for E- and H-field distributions for the entire coupled region consisting of the shaped radiator (using CAD files) as well as the model of the human head.

Even though most of the focus in the past has been on safety compliance testing, these numerical techniques are now beginning to be used for important diagnostic and therapeutic applications (51, 52). Some examples of therapeutic applications are designs of implantable and noninvasive devices such as pace makers; defibrillators; and applicators for hyperthermia, hypothermia, and transcranial magnetic stimulation. Examples of diagnostic applications include detection of breast cancer and regions of abnormal electrical activity for the brain and the heart amongst many others.

The *Annual Review of Biomedical Engineering* is online at http://bioeng.annualreviews.org

LITERATURE CITED

1. IEEE Std. C95.1. 1999. *IEEE Standard for Safety Levels With Respect to Human Exposure to Radiofrequency Electromagnetic Fields, 3 kHz to 30 GHz*. New York: IEEE
2. ICNIRP. 1998. Guidelines for limiting exposure to time-varying electric, magnetic and electromagnetic fields. *Health Phys.* 74(4):494–522
3. US FCC. 1996. Guidelines for evaluating the environmental effects of radiofrequency radiation. FCC 96-326
4. Gandhi OP. 1995. Some numerical methods for EM dosimetry: ELF to microwave frequencies. *Radio Sci.* 30:161–77
5. Gandhi OP, Lazzi G, Furse CM. 1996. Electromagnetic absorption in the human head and neck for mobile telephones at 835 and 1900 MHz. *IEEE Trans. Microw. Theory Tech.* 44:1884–97
6. Okoniewski M, Stuchly MA. 1996. A study of the handset antenna and human body interaction. *IEEE Trans. Microw. Theory Tech.* 44:1855–64
7. Taflove A, Brodwin ME. 1975. Numerical solution of steady-state electromagnetic scattering problems using the time-dependent Maxwell's equations. *IEEE Trans. Microw. Theory Tech.* 23:623–30
8. Spiegel RJ, Fatmi MB, Kunz KS. 1985. Application of a finite-difference technique to the human radio-frequency dosimetry problem. *J. Microw. Power* 20:241–54
9. Sullivan DM, Gandhi OP, Taflove A. 1988. Use of the finite-difference time-domain method in calculating EM absorption in man models. *IEEE Trans. Biomed. Eng.* 35: 179–86
10. Chen, JY, Gandhi OP. 1991. Currents induced in an anatomically-based model of a human for exposure to vertically polarized electromagnetic pulses. *IEEE Trans. Microw. Theory Tech.* 39:31–39
11. Gandhi OP, Chen JY. 1991. Numerical dosimetry at power-line frequencies using anatomically based models. *Bioelectromagn. Suppl.* 1:43–60
12. Kunz KS, Luebbers RJ. 1993. *The Finite-Difference Time-Domain Method*. Boca Raton, FL: CRC. 448 pp.
13. Taflove A, Hagness SC. 2000. *Computational Electrodynamics: The Finite-Difference* Time-Domain Method. Norwood, MA: Artech House. 852 pp. 2nd ed.
14. Gao BQ, Gandhi OP. 1992. An expanding-grid algorithm for the finite-difference time-domain method. *IEEE Trans. Electromagn. Compat.* 34:277–83
15. Gandhi OP, Wu D, Chen JY, Conover DL. 1997. Induced current and SAR distributions for a worker model exposed to an RF dielectric heater under simulated workplace conditions. *Health Phys.* 72:236–42
16. Wiart J, Chaillou S, Drago S. 1997. Calculation of the power absorbed by the head using a nonuniform FDTD. *Proc. N. Am.*

Radio Sci. Meet., Montreal, Canada. 772 pp.
17. Tinniswood AD, Lazzi G, Gandhi OP. 1999. The use of the expanding-grid FDTD method for simulation of CAD-derived personal wireless telephones. *Microw. Opt. Tech. Lett.* 22:24–29
18. Okoniewski M, Okoniewska E, Stuchly MA. 1997. Three-dimensional subgridding algorithm for FDTD. *IEEE Trans. Antennas Propag.* 45:422–29
19. Armitage DW, LeVeen HH, Pethig R. 1983. Radiofrequency-induced hyperthermia: computer simulation of specific absorption rate distribution using realistic anatomical models. *Phys. Med. Biol.* 28:31–42
20. Gandhi OP, DeFord JF, Kanai H. 1984. Impedance method for calculation of power deposition patterns in magnetically induced hyperthermia. *IEEE Trans. Biomed. Eng.* 31:644–51
21. DeFord JF, Gandhi OP. 1985. An impedance method to calculate currents in biological bodies exposed to quasi-static electromagnetic fields. *IEEE Trans. Electromagn. Compat.* 27:168–73
22. Gandhi OP, DeFord JF. 1988. Calculation of EM power deposition for operator exposure to RF induction heaters. *IEEE Trans. Electromagn. Compat.* 30:63–68
23. Orcutt N, Gandhi OP. 1990. Use of the impedance method to calculate 3-D power deposition patterns for hyperthermia with capacitive plate electrodes. *IEEE Trans. Biomed. Eng.* 37:36–43
24. Gandhi OP, Chen JY. 1992. Numerical dosimetry at power line frequencies using anatomically-based models. *Bioelectromagn. Suppl.* 1:43–60
25. Baraton P, Hutzler B. 1995. Magnetically-induced currents in the human body. *IEC Technol. Trend Assess.*
26. Furse CM, Gandhi OP. 1998. Calculations of electric fields and currents induced in a millimeter-resolution human model at 60 Hz using the FDTD method. *Bioelectromagnetics* 19:293–99
27. Dawson TW, Stuchly MA. 1998. High resolution organ dosimetry for human exposure to low frequency magnetic fields. *IEEE Trans. Magn.* 34:708–18
28. Dimbylow PJ. 1998. Induced current densities from low-frequency magnetic fields in a 2 mm resolution, anatomically realistic model of the body. *Phys. Med. Biol.* 43:221–30
29. Dawson TW, Caputa K, Stuchly MA. 1999. Numerical evaluation of 60 Hz magnetic induction in the human body in complex occupational environments. *Phys. Med. Biol.* 44:1025–40
30. Gustrau F, Bahr A, Rittweger M, Goltz S, Eggert S. 1999. Simulation of induced current densities in the human body at industrial induction heating frequencies. *IEEE Trans. Electromagn. Compat.* 41:480–86
31. Stuchly MA, Dawson TW. 2000. Interaction of low-frequency electric and magnetic fields with the human body. *Proc. IEEE* 88:643–64
32. Gandhi OP, Kang G, Wu D, Lazzi G. 2001. Currents induced in anatomic models of the human for uniform and nonuniform power frequency magnetic fields. *Bioelectromagnetics* 22:112–21
33. Gandhi OP, Kang G. 2001. Calculation of induced current densities for humans by magnetic fields of electronic article surveillance devices. *Phys. Med. Biol.* 46:2759–71
34. Harris C, Boivin W, Boyd S, Coletta J, Kerr L, et al. 2000. Electromagnetic field strength levels surrounding electronic article surveillance (EAS) systems. *Health Phys.* 78:21–27
35. European Std. EN50357. 2001. Evaluation of human exposure to EM fields from devices used in electronic article surveillance (EAS), radiofrequency identification (RFID) and similar applications. Brussels, Belgium: CENELEC-Eur. Comm. Electrotech. Stand.
36. Dimbylow PJ, Mann SA. 1994. SAR calculations in an anatomically-based realistic model of the head for mobile communication transceivers at 900 and 1800 MHz. *Phys. Med. Biol.* 39:1537–53

37. Jensen MA, Rahmat-Samii Y. 1995. EM interaction of handset antennas and a human in personal communication. *Proc. IEEE* 83:7–17
38. Gandhi OP, Chen JY. 1995. Electromagnetic absorption in the human head from experimental 6-GHz handheld transceivers. *IEEE Trans. Electromagn. Compat.* 37:547–58
39. Watanabe S, Taki M, Nojima T, Fujiwara O. 1996. Characteristics of the SAR distributions in a head exposed to electromagnetic fields radiated by a handheld portable radio. *IEEE Trans. Microw. Theory Tech.* 44:1874–83
40. Tinniswood AD, Furse CM, Gandhi OP. 1998. Computations of SAR distributions for two anatomically based models of the human head using CAD files of commercial telephones and the parallelized FDTD code. *IEEE Trans. Antennas Propag.* 46(6): 829–33
41. Gandhi OP, Lazzi G, Tinniswood A, Yu Q-S. 1999. Comparison of numerical and experimental methods for determination of SAR and radiation patterns of handheld wireless telephones. *Bioelectromagn. Suppl.* 4:93–101
42. Bernardi P, Cavagnaro M, Pisa S, Piuzzi E. 2000. Human exposure to radio base-station antennas in urban environment. *IEEE Trans. Microw. Theory Tech.* 48: 1996–2002
43. Wang J, Fujiwara O. 2000. Dosimetry analysis and safety evaluation of realistic head models for portable telephones. *Trans. IEICE* J83-B(5):720–25
44. Lentner C. 1984. *Geigy Scientific Tables 3*. Basel, Switz.: CIBA-GEIGY
45. Olsen RG, Griner TA. 1989. Outdoor measurements of SAR in a full-size human model exposed to 29.2 MHz near-field irradiation. *Bioelectromagnetics* 10:162–71
46. Gandhi OP, Lam MS. 2002. An on-site dosimetry system for safety assessment of wireless base stations using spatial harmonic components. *IEEE Trans. Antennas Propag.* 50: In press
47. Balzano Q, Garay O, Manning TJ Jr. 1995. Electromagnetic energy exposure of simulated users of portable cellular telephones. *IEEE Trans. Veh. Tech.* 44:390–403
48. Schmid T, Egger O, Kuster N. 1996. Automated E-field scanning system for dosimetric assessments. *IEEE Trans. Microw. Theory Tech.* 44:105–13
49. Yu Q, Gandhi OP, Aronsson M, Wu D. 1999. An automated SAR measurement system for compliance testing of personal wireless devices. *IEEE Trans. Electromagn. Compat.* 41(3):234–45
50. Hartsgrove G, Kraszewski A, Surowiec A. 1987. Simulated biological materials for electromagnetic absorption studies. *Bioelectromagnetics* 8:29–36
51. Hagness SC, Taflove A, Bridges JE. 1999. Three-dimensional FDTD analysis of a pulsed microwave confocal system for breast cancer detection: design of an antenna-array element. *IEEE Trans. Antennas Propag.* 47(5):783–91
52. Lazzi G, DeMarco SC, Liu W, Humayun M. 2001. Simulated temperature increase in a head-eye model containing an intraocular retinal prosthesis. *IEEE Int. Symp. Antennas Propag. Soc. Abstr.* 2:72–75

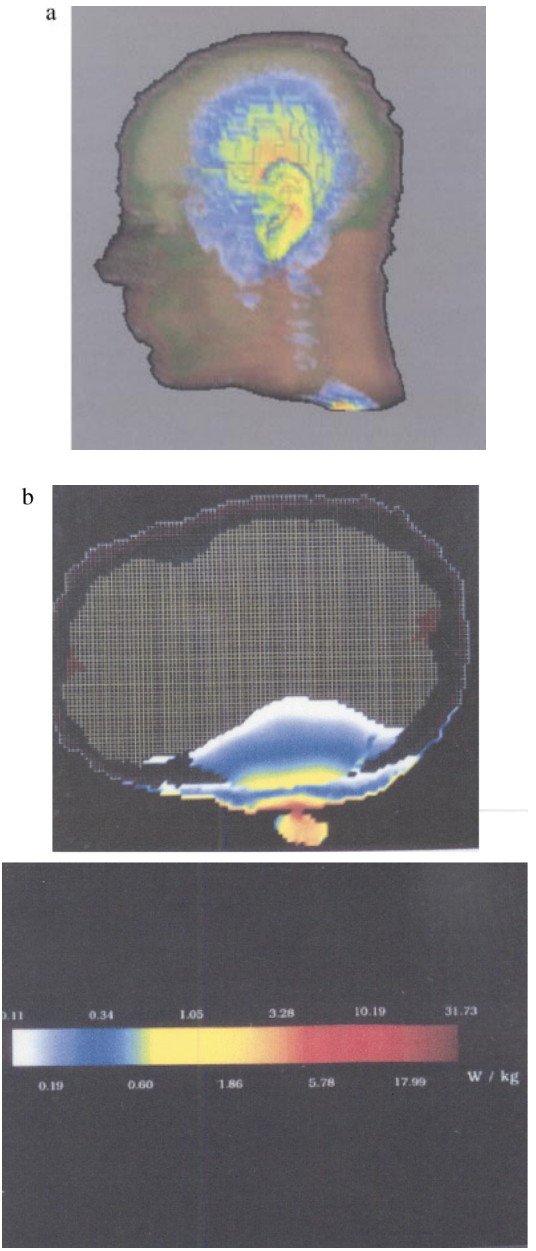

Figure 2 A typical SAR distribution for a cellular telephone radiating at 835MHz. Shown here: (*a*) the side of the head exposed to the cellular telephone; (*b*) a horizontal cross section of the head.

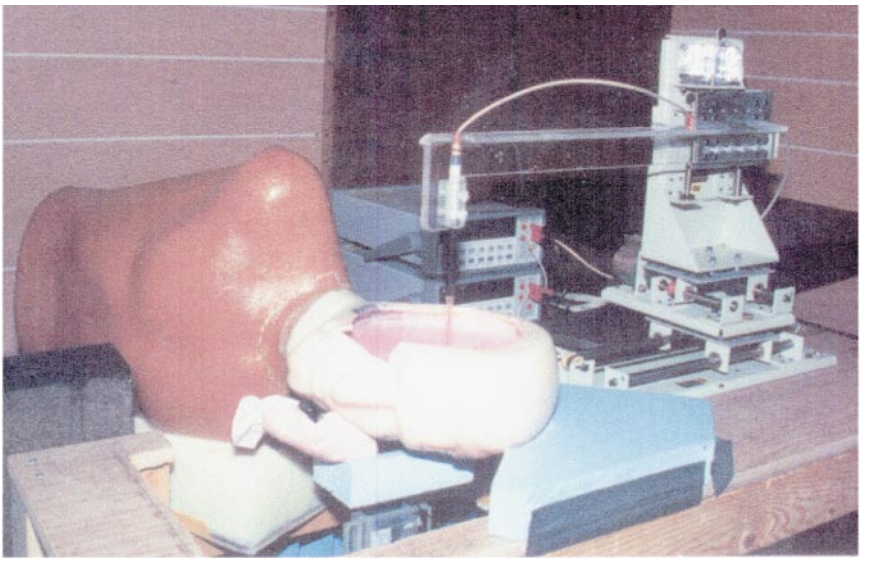

Figure 8 The 3-D stepper-motor-driven automated SAR measurement system.